Li/Na Ion Intercalation Process into Sodium Titanosilicate as Anode Material

Jingyuan Liu,[a] Yao Liu,[a] Yonggang Wang,[a] Congxiao Wang,[a] and Yongyao Xia*[a, b]

A natisite structured material, Na_2TiSiO_5, has been investigated as anode for lithium- and sodium-ion batteries. The results show that Na_2TiSiO_5 can deliver a capacity of 260 mAh g^{-1} with good reversibility when used as anode in Li-ion batteries. In contrast to the conversion reaction mechanism observed for its analogue Li_2TiSiO_5, a solid-solution type intercalation mechanism is found for the lithiation/delithiation process of Na_2TiSiO_5.

Lithium intercalation occurs through a three-dimensional diffusion path after crossing an energy barrier around 1.0 eV. Sodium-ions could only migrate through a one-dimensional channel after overcoming a much higher energy barrier of 1.8 eV, which solely delivers a reversible capacity of 40 mAh g^{-1} for sodium-ion storage.

1. Introduction

Lithium-ion batteries (LIB) dominate the application of portable electronic devices and electric vehicles.[1–6] Graphite has been the mainstream anode material since the birth of lithium-ion batteries. But its lithium intercalation potential is too close to lithium plating potential, thus makes it easy to form lithium dendrite and raise safety concerns.[7–10] Titanium-based anode materials, such as lithium titanate and titanium oxide (including anatase and bronze species), perform a higher working potential above 1.5 V *vs.* Li$^+$/Li by involving a redox couple of Ti^{4+}/Ti^{3+},[11–14] thus reduce the safety risk. However, this potential restricts output voltage of the full cell, especially if a cell adopts some low potential cathode, like LiFePO$_4$.[15,16] To extricate the dilemma, we introduced a polyanionic anode material, Li_2TiSiO_5 in our previous work. By introducing redox couple of Ti^{4+}/Ti^{2+}, a proper lithiation potential of 0.28 V *vs.* Li$^+$/Li has been achieved, which ensures the energy density, but avoids potential risk of lithium plating. In addition, benefited from the firm structure of titanosilicate, Li_2TiSiO_5 displays excellent reversibility.[17,18]

The application of Li_2TiSiO_5 reveals some superiority of polyanionic materials as electrodes, such as high reversibility and high capacity. But until now, no matter in the field of lithium or sodium ion electrode, most of the reported polyanionic materials are cathodes, such as LiFePO$_4$,[19]

LiMnPO$_4$,[20] LiCoPO$_4$,[21] Li_2FeSiO_4,[22] LiFeBO$_3$[23] and Na$_3$V$_2$(PO$_4$)$_3$.[24] Besides LiTi$_2$(PO$_4$)$_3$ and NaTi$_2$(PO$_4$)$_3$, which are commonly used in aqueous battery,[25,26] there are very few reports about polyanionic anode materials. One example, Vittorio Luca *et al.* reported that Na$_2$Ti$_2$O$_3$SiO$_4$·2.76H$_2$O as an anode of lithium-ion batteries and it delivers a capacity of 180–200 mAh g^{-1}.[27] Recently, Liu *et al.* expanded the material's application to sodium ion batteries (SIB).[28] However, the crystal water and proton in this material hinders its electrochemical performance not only by reducing its capacity but also restricting the material's reversibility. And it has been noticed that the other non-water crystallized sodium titanosilicate material, Na_2TiSiO_5, which is an analogue of the former reported Li_2TiSiO_5, has never been reported as the anode material for neither lithium-ion nor sodium-ion batteries.

Herein, we have explored a new natisite anode material, Na_2TiSiO_5, which has a very similar crystal structure with Li_2TiSiO_5. The material's lithiation and sodiation properties have been investigated in this work. Na_2TiSiO_5 exhibits a reversible capacity of 260 mAh g^{-1} as lithium anode, accompanied by the redox couple Ti^{4+}/Ti^{2+}. Moreover, this work proves a solid-solution typed lithium intercalation mechanism of Na_2TiSiO_5 material, which is very different from conversion typed mechanism of Li_2TiSiO_5. And bond valence sum method demonstrates that, during intercalation, Na_2TiSiO_5 provides a three-dimensional lithium ion diffusion path, with an energy barrier around 1.0 eV. In addition, Na_2TiSiO_5 exhibits the ability to store sodium ion, but with a less capacity of about 40 mAh g^{-1}. The result of galvanostatic intermittent titration technique shows that kinetics limitation on sodium ion diffusion restricts its performance as a sodium-ion battery anode.

[a] Dr. J. Liu, Dr. Y. Liu, Prof. Y. Wang, Prof. C. Wang, Prof. Y. Xia
Department of Chemistry and Shanghai Key Laboratory of Molecular Catalysis
Institute of New Energy and Innovative Materials
Institute of New Energy, iChEm (Collaborative Innovation Center of Chemistry for Energy Materials)
Fudan University
Shanghai, 200433, P. R. China
E-mail: yyxia@fudan.edu.cn
[b] Prof. Y. Xia
College of Chemistry and Molecular Engineering
Zhengzhou University
Zhengzhou 450001, P. R. China

2. Results

2.1. Material Characterization

Powder X-Ray diffraction was used to determine the structural properties of synthesized Na_2TiSiO_5. The Rietveld refinement result of Na_2TiSiO_5 shows that it is pure-phased and has a similar crystal structure with Li_2TiSiO_5, both belong to space group P4/nmm. Moreover, the refinement result reveals that Na_2TiSiO_5 and Li_2TiSiO_5 even have almost the same lattice parameter along a and b axis (see Figure 1 and Figure S1, Table S1 and S2). But Na_2TiSiO_5 lattice is 15.7% expanded along the c axis, causing a 17.5% expansion of lattice volume than Li_2TiSiO_5. They both have a layered structure with Li^+ or Na^+ fully occupying the $4d$ site. LiO_6 or NaO_6 octahedra layer and TiO_6 octahedra / SiO_4 tetrahedra layer appear alternately along the c axis, where TiO_6 octahedra are distorted with one Ti–O bond stretched.

The synthesized Na_2TiSiO_5 is irregularly shaped bulk, with most of the particles around 1 μm (Figure S2). Due to the instability of natisite Na_2TiSiO_5 under high temperature,[29] the synthesized Na_2TiSiO_5 wasn't coated by a conductive carbon layer. And Energy-dispersive X-ray spectroscopy (EDS, Figure S3) shows that all elements in synthesized Na_2TiSiO_5 are homogeneously distributed, further confirms this material contains none impurities.

2.2. Electrochemical Performance

The electrochemical activity of Li_2TiSiO_5 encourages further exploration of lithium and sodium storage performance on its analogue, Na_2TiSiO_5. Discharge-charge profiles of Na_2TiSiO_5 as LIB and SIB anode are shown in Figure 2a and 2c. One most obvious is that its sodium ion storage capacity is far less than lithium ion. Under current density of 0.01 $A\,g^{-1}$, as LIB anode, Na_2TiSiO_5 performs a reversible capacity of 260 $mAh\,g^{-1}$.

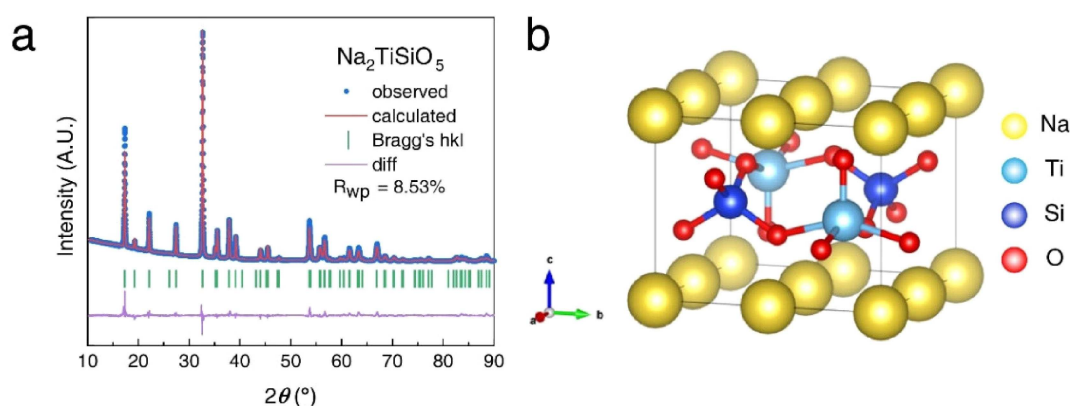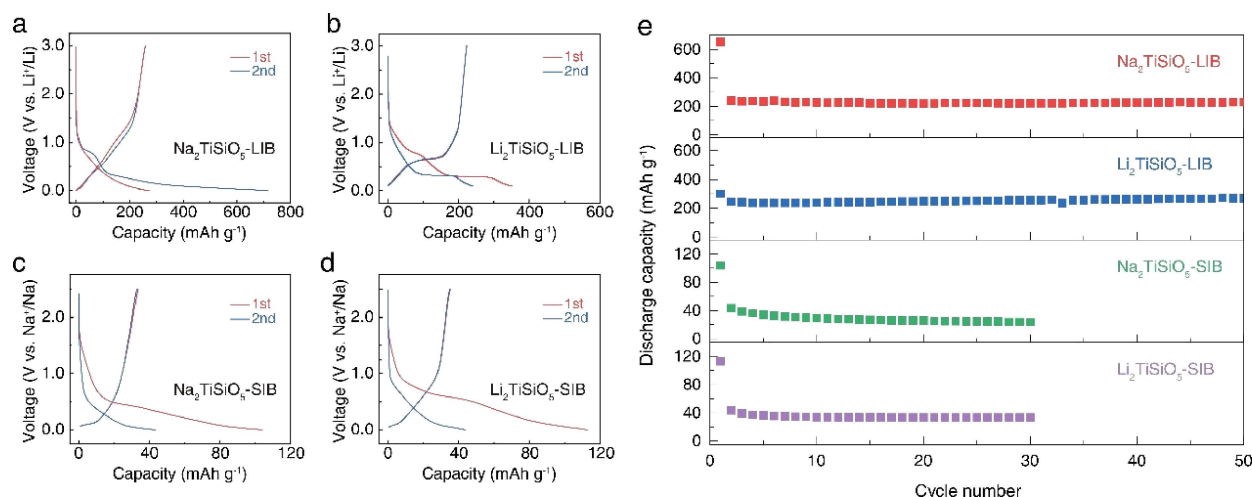**Figure 1.** a) The Rietveld refinement of the X-ray diffraction pattern of Na_2TiSiO_5 and b) illustration of a unit cell.

Figure 2. First and second cycles' discharge and charge profiles of Na_2TiSiO_5 as anode of a) LIB and c) SIB, with testing potential windows of 0.0–3.0 V vs. Li^+/Li and 0.0-2.5 V vs. Na^+/Na, respectively. And discharge and charge profiles of Li_2TiSiO_5 as anode of b) LIB and d) SIB, with testing potential windows of 0.1–3.0 V vs. Li^+/Li and 0.0–2.5 V vs. Na^+/Na, respectively. e) The cyclic ability of Na_2TiSiO_5 and Li_2TiSiO_5 as anode of LIB and SIB. All characterizations of the figure displayed were carried out by CR2032 coin-type half-cell, with polished lithium or sodium metal foil as counter-electrode. a)–d) adopted a very low current density of 0.01 $A\,g^{-1}$ to fulfill the material's performance and e) adopted a current density of 0.02 $A\,g^{-1}$

Calculated from this capacity, the valence of Ti changes from Ti^{4+} to Ti^{2+} during the discharge process (the theoretical capacity involving redox couple Ti^{4+}/Ti^{3+} and Ti^{4+}/Ti^{2+} are 132.7 mAh g^{-1} and 265.3 mAh g^{-1}, respectively). However, only a reversible capacity of 43 mAh g^{-1} is observed when Na_2TiSiO_5 severs as SIB anode. Irreversible capacity also observed in both systems. For lithium storage performance, the irreversible capacity rises from the decomposition of electrolyte.[30,31] Compared to discharge and charge profiles of Li_2TiSiO_5 as LIB anode (Figure 2b), Na_2TiSiO_5 exhibits a complete slope curve, indicating that a process different from Li_2TiSiO_5 occurs during Na_2TiSiO_5 lithiation stage. And as SIB anode, there is no obvious distinction found between Na_2TiSiO_5 and Li_2TiSiO_5 (Figure 2c and 2d). Cycling performance of both Na_2TiSiO_5 and Li_2TiSiO_5 as anode of LIB and SIB has been tested on coin typed half-cell under a current density of 0.02 A g^{-1}, and shown in Figure 2e. The good reversibility of Li_2TiSiO_5 as LIB anode verifies former report on its performance.[17] When serving as LIB anode, Na_2TiSiO_5 also retains good reversibility. Despite the irreversible capacity from the initial cycle, there is capacity retention of 229.1 mAh g^{-1} (95% of the second cycle) after 50 cycles. While both materials experience a continuously capacity decay when they serve as SIB anode. After 30 cycles' discharging/charging, remained capacity of Na_2TiSiO_5 and Li_2TiSiO_5 were 23.7 mAh g^{-1} and 33.4 mAh g^{-1}, respectively, which are much less than capacity of the second cycle (both of them are about 43 mAh g^{-1}). Due to the absence of conductive coating material, Na_2TiSiO_5 performances a relatively worse rate performance even as LIB anode (Figure S4). Under a current density of 0.2 A g^{-1} ($\sim$0.8 C), a discharge capacity of 135.9 mAh g^{-1} was observed. And under overwhelm high current density of 3 A g^{-1} ($\sim$11.5 C), the discharge capacity slumps to 29.8 mAh g^{-1}, only 11.5% of theoretical capacity. Techniques allowing low temperature coating of conducting species, e.g. conducting polymers, may help to alleviate the capacity decay under high current density.

3. Discussion

3.1. Lithium Storage Mechanism

As mentioned above, the difference between Na_2TiSiO_5 and Li_2TiSiO_5 discharge/charge profile as LIB anode implies different lithium storage mechanisms between these two materials. Since the lithiation mechanism of Li_2TiSiO_5 has been revealed by the former work, in this part we mainly focus on the lithiation mechanism of Na_2TiSiO_5. In-situ XRD was first applied to Na_2TiSiO_5 electrodes. As reported before, during cycling peaks belonging to Li_4SiO_4 and TiO emerge and fade on Li_2TiSiO_5 ex-situ XRD patterns, thus proves the conversion storage mechanism of Li_2TiSiO_5. However, in the case of Na_2TiSiO_5, we didn't see any new peak appearing/disappearing or peak shift during the material's lithiation/delithiation process (Figure 3a), this phenomenon indicates the lattice structure change might be negligible in the investigated process. To further investigate possible lithium host site, Maximum entropy

method (MEM) combined Rietveld refinement was applied to look over the Na_2TiSiO_5 crystal structure. MEM is an effective method in revealing nuclear/charge density distribution within crystals. And the result is very helpful in analyzing vacancy and ion diffusion path inside the lattice.[32–37] In this case, charge distribution contour was generated by MEM based on XRD refinement result. It reveals that the 4e site is the most possible place to host lithium ions (Figure 3c). One would be noticed that the vacancy of 4e site in Na_2TiSiO_5 is larger than the one inside Li_2TiSiO_5, the volume of the vacancy-oxygen octahedron in Na_2TiSiO_5 is 20% expanded than in Li_2TiSiO_5, it could possibly be the reason causing different lithiation mechanism between these two materials. To identify structure evolution, we adopted ex-situ XRD and accompanied refinement to explore lattice parameter change during discharge/charge. The XRD accompanied refinement has been proved as an effective method, including "zero strain" materials which has minute lattice parameter change during ion intercalation.[38–43] XRD refinement results of electrode under various discharge/charge states provide more details of Na_2TiSiO_5 lattice structural change. As shown in Figure S5, electrodes were extracted from cell when discharged/charged to certain states (3.0 V, discharged down to 0.7 V, 0.5 V, 0.3 V, 0.1 V, 0 V and recharged back to 0.1 V, 0.3 V, 0.5 V, 0.7 V and 3.0 V) and their XRD patterns were collected under inert gas atmosphere protection. Their refinement result was summarized in Figure 3b. During cycling, lattice parameters remain stable, the maximum volume expansion occurring at 0 V is 0.53%. The refinement result also indicates that during discharge process, lithium occupancy at 4e site increases and then decreases following charge process. And lithium/titanium occupancy at various states conforms well to capacities observed from the experiment, which verifies the validity of refinement results (Figure S6 and Table S3). All these results combined prove a solid-solution typed intercalation mechanism during lithiation and delithiation process of Na_2TiSiO_5. Lithium ions are reversibly intercalated into the 4e site of Na_2TiSiO_5 lattice, leading to a slight expansion of lattice structure in a and c axis. But, overall, the volume change during this process is negligible.

The intercalation mechanism of Na_2TiSiO_5 leads to a stable discharge-charge profile during cycling. In contrast, Li_2TiSiO_5 suffers from profile variation, which is resulted from the conversion reaction caused pulverization (Figure S7). To quantify the stability of discharged and charged profile, the average potential of two materials during discharge and charge is calculated by Equation (1):

$$V_{average} = \int_{C_2}^{C_1} V \, dC \, / \, C \tag{1}$$

Where $V_{average}$ is the calculated average potential, C_1 and C_2 are discharged/charged capacity at the beginning/end, C is the capacity of Na_2TiSiO_5/Li_2TiSiO_5. The results were summarized in Figure S8, and it is clearly found that, no matter on discharge or charge stage, the average potential change in Na_2TiSiO_5 is smaller than Li_2TiSiO_5. After 30 cycles, average potential changes of 0.10 V and 0.13 V are found in Na_2TiSiO_5 discharge
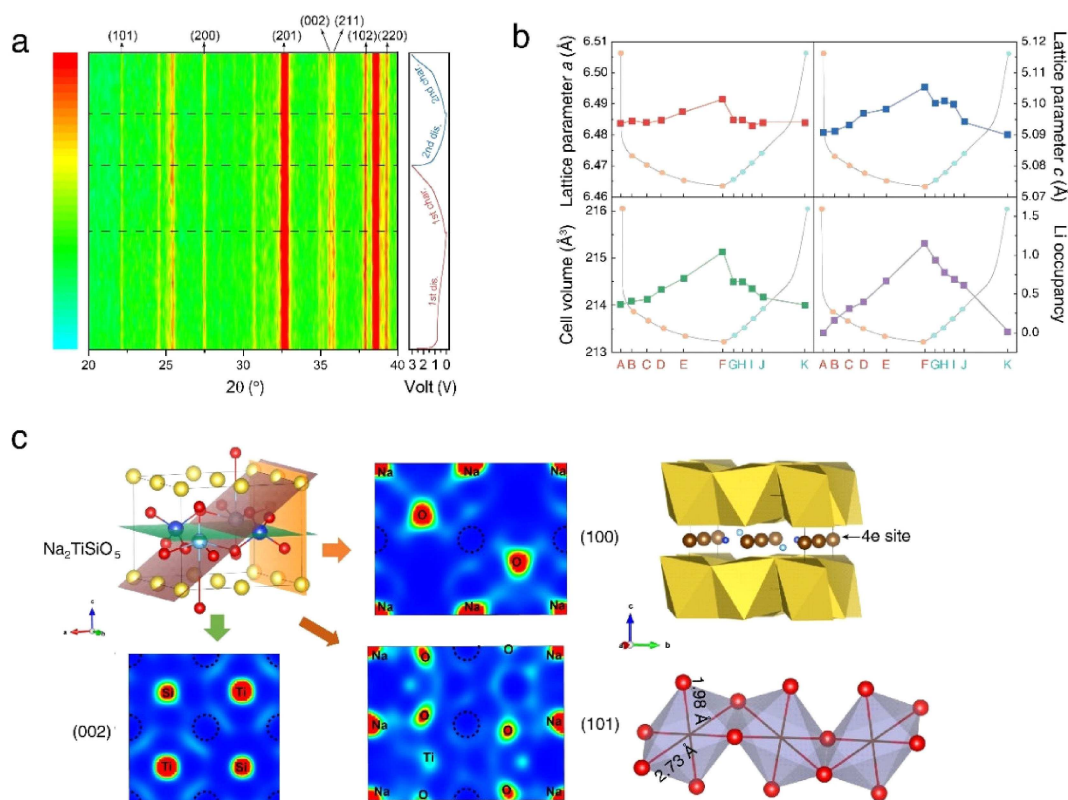
Figure 3. a) In-situ XRD pattern of Na_2TiSiO_5 electrodes during lithiation and delithiation process at first and second cycle, with time-voltage profile combined on the right. Intensity of each peak was presented by colors. b) Refinement result of each discharge/charge state based on ex-situ XRD patterns. The tested states included in the figures are: A: initial state (3.0 V), B: discharged down to 0.7 V, C: discharged down to 0.5 V, D: discharged down to 0.3 V, E: discharged down to 0.1 V, F: discharged down to 0.0 V, G: recharged back to 0.1 V, H: recharged back to 0.3 V, I: recharged back to 0.5 V, J: recharged back to 0.7 V and K: recharged back to 3.0 V. The top-left and top right display lattice parameters *a* and *c* of the lattice under various states, bottom-left displays lattice volume of the lattice under test states and bottom-right shows Li ion occupancy under each state. All refinement result figures contain an illustrated time-voltage profile with tested states labeled on it. c) The left displays MEM calculated charge distribution result of the Na_2TiSiO_5 lattice, with section on (100), (002) and (101) faces displayed. The right-top shows position of 4*e* site (brown ball) within a Na_2TiSiO_5 unit cell and the right-bottom illustrates the size and connections of 4*e* vacancy-oxygen octahedra.

and charge profile, respectively. Also, one should be noticed that, after the initial 5 cycles, the average potential almost stays stable. In contrast, the average potential of Li_2TiSiO_5 increased to 0.20 V (discharge) and 0.16 V (charge) higher than original.

3.2. Kinetic Study of Lithium- and Sodium-Ion Intercalation

It is also interesting to investigate the kinetics during lithium/sodium ion intercalating/de-intercalating, to explore the reason which causes capacity difference when various ions are intercalated. The Bond Valence Energy Landscapes (BVEL) method was adopted to achieve this task. This methodology is developed by S. Adams, who defined the soft bond valence parameters as well.[44,45] This method derives from Bond Valence Sum (BVS) method, which is applied to analyzing bond lengths of crystal structure. The BVEL method has been used as a simple tool to analyze the route and dimensionality of diffusion paths and has already been applied for lithium or sodium conduction route in several reports.[46–48] By adopting BVEL into this case, both the diffusion barrier of lithium/sodium ion and their diffusion path is possible to be obtained. Firstly, BVEL

method is performed on two structures, $Na_2^{4d}Li_{0.5}^{4e}TiSiO_5$ and $Na_2^{4d}Na_{0.5}^{4e}TiSiO_5$, respectively, and the obtained migration maps are shown in Figure 4a, b and Figure S9. In a migration map, a selected isosurface represents the maximum ion diffusion area according to a chosen energy above the minimum energy (the zero of energy), where the chosen energy is recognized as activation energy. And the minimum activation energy which leads to an uninterruptedly isosurface crossing the unit cell would be treated as the energy barrier when lithium migrates following the path illustrated by the isosurface. Migration map of lithium-ion with isosurfaces corresponding to 0.5 eV, 1.0 eV and 1.1 eV activation energy is displayed in Figure 4a. And to our surprise, instead of merely diffusing between layers, the lithium ion could also migrate cross the NaO_6 layer, thus exhibits a three-dimensional diffusion path under a chosen activation energy of 1.1 eV. To make a clearer exhibition, three views of migration map with activation energy of 1.3 eV has also been displayed in Figure S9, where zig-zag diffusion paths of lithium ions are explicitly drawn. Moreover, the energy barriers of lithium ion migration are calculated, it comes out with a very closed barrier crossing (0.990 eV) and along (1.058 eV) the NaO_6 layer (Figure 4e and
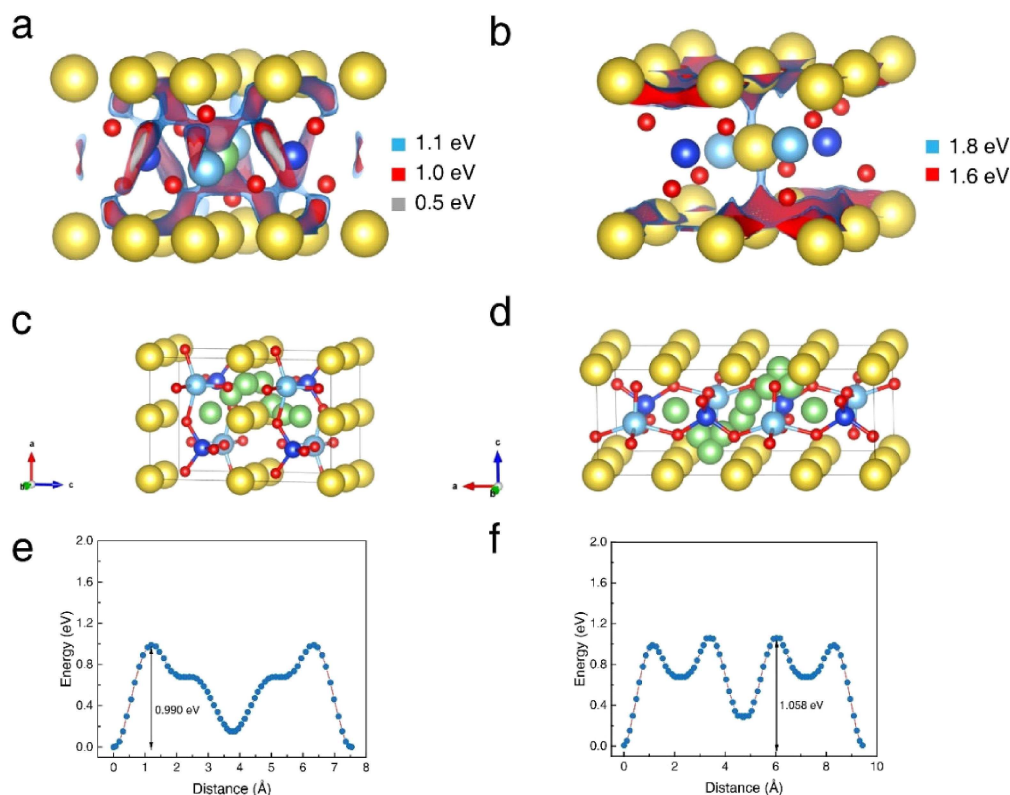
Figure 4. BVEL of Na_2TiSiO_5 considering a) lithium ion diffusion and b) sodium ion diffusion. The isosurfaces of lithium ion migration paths are plotted in red, blue and grey according to activation energies of 1.1 eV, 1.0 eV and 0.5 eV, presenting 3D diffusion, 1D diffusion and blocked diffusion, respectively. Isosurfaces of sodium ion paths are plotted as red and blue for activation energies of 1.8 eV and 1.6 eV, presenting 1D diffusion and blocked diffusion. Illustration of lithium migration path in Na_2TiSiO_5 along c) c-axis and d) a-axis, and e), f) the energy barriers corresponding to each path. To draw a full length of the diffusion path, two unit cells along the diffusing axis are illustrated.

4 f), which further proves the three-dimensional diffusion property of lithium ion in Na_2TiSiO_5 structure (Figure 4c and 4d). However, in the case of sodium diffusing (displayed in Figure 4b), sodium ion could only diffuse along a one-dimensional path crossing the NaO_6 layer, with a much higher activation energy of 1.8 eV. It means that sodium ion faces a larger barrier than lithium-ion when it migrates within the Na_2TiSiO_5 lattice. The result of BVEL proves that it is much more difficult for sodium than lithium to diffuse within Na_2TiSiO_5 crystal structure, as a consequence, limiting the sodium storage capacity.

Activation energy obtained from BVEL reflects Li/Na migration behavior within an infinite and defect-less single crystal, furthermore, in order to provide evidence from an experimental aspect and combine other possibly kinetic affection, galvanostatic intermittent titration technique (GITT) has been used to investigate the lithium/sodium diffusion coefficients. By GITT, the diffusion coefficient can be calculated based on chronopotentiometry at nearly thermodynamic equilibrium conditions. The D_{M^+} is calculated by Equation (2):

$$D_{M^+} = \frac{4}{\pi}\left(\frac{m_B V_m}{M_B S}\right)^2 \left(\frac{\Delta E_s}{\tau(dE_\tau/d\sqrt{\tau})}\right)^2 (\tau \ll \frac{L^2}{D_{M^+}}) \qquad (2)$$

Where m_B is the mass of active electrode material, V_m is the molar volume and M_B is molecular weight of samples. S is the area of the electrode, and τ is the time duration during the current pulse, and ΔE_s is the difference in the steady-state voltage at a single-step GITT. L is the diffusion length of M^+ ions. In equation (2), $dE_\tau/d\sqrt{\tau}$ is difficult to be obtained thus making an obstacle in practical use. And if the cell potential (E) has a linear relation to $\tau^{1/2}$, equation 2 can be simplified as Equation (3):[49,50]

$$D_{M^+} = \frac{4}{\pi\tau}\left(\frac{m_B V_m}{M_B S}\right)^2 \left(\frac{\Delta E_s}{\Delta E_\tau}\right)^2 (\tau \ll \frac{L^2}{D_{M^+}}) \qquad (3)$$

The GITT curve of lithium/sodium intercalating Na_2TiSiO_5 has been displayed in Figure 5a and 5b. To avoid the affection of initial irreversible capacity, the GITT was taken on the third cycle's discharge curve. Discharge current densities for both lithium and sodium discharge are 0.02 A g^{-1}. And tested potential ranges are 0 V–3 V vs. Li$^+$/Li and 0 V–2.5 V vs. Na$^+$/Na, respectively. For lithium intercalation, each galvanostatic current step is performed for 30 min and then followed an interval rest of 60 min to reach a nearly steady state. However, to reach a steady state for sodium discharged Na_2TiSiO_5, it needs a shorted galvanostatic stage of 20 min and a longer rest period of 120 min. In Figure S10a and S10c, typical GITT profiles
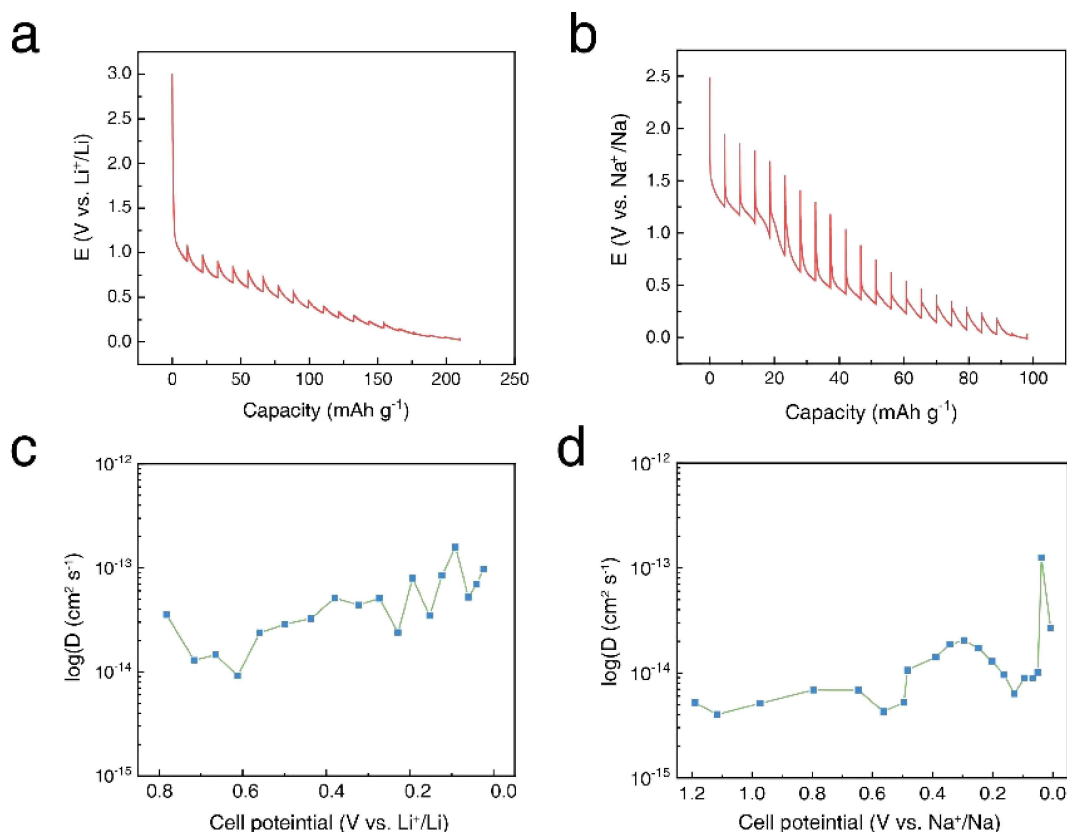
Figure 5. Discharge capacity versus potential curve of Na_2TiSiO_5 when it stores a) lithium ion and b) sodium ion in GITT process, and diffusion coefficients of c) lithium ion and d) sodium ion as a function of potential.

during a single-step are displayed for both two systems, and Figure S10b and S10d proves the linear relation of E and $\tau^{1/2}$. As a result, the simpler equation (3) can be used in this case. The calculated ionic diffusion coefficient is included in Figure 5c and 5d. It is clear that lithium has a larger diffusion coefficient. It is also worthy to notice that under GITT method (which the capacity can be treated as the material's thermodynamic capacity), the capacity of lithium storage in Na_2TiSiO_5 has no significant difference from the galvanostatic discharge process. However, after a full relaxation, the capacity of sodium storage becomes more than two times compared to galvanostatic discharge, this fact further proves the kinetic difficulty for sodium ion to be intercalated into the Na_2TiSiO_5 lattice. Namely, combining both BVEL and GITT results, it has been proved that instead of thermodynamic limitation, the bottleneck of Na_2TiSiO_5 low sodium storage capacity arises from its slow kinetic behavior when sodium is intercalated, and it is one important reason contributes to kinetic limitation that the sodium ion's restrained migration within Na_2TiSiO_5 lattice due to the one-dimension diffusion path and high energy barrier.

4. Conclusion

In this work, for the first time, Na_2TiSiO_5 has been proved as a proper anode of lithium-ion batteries. A reversible capacity of 260 mAh g^{-1} and good reversibility has been achieved. This

capacity determines that the redox couple of Ti^{4+}/Ti^{2+} is involved during the discharge/charge process. Also, it has been proved a solid solution typed intercalation mechanism occurs during Na_2TiSiO_5 lithiation, and a three-dimensional diffusion path has been found with an energy barrier around 1.0 eV. Furthermore, sodium storage performance of this material has been investigated in this work as well. BVEL and GITT prove that kinetics limitation of sodium diffusion in Na_2TiSiO_5 crystal structure limits the capacity of Na_2TiSiO_5 storing Na^+.

Acknowledgement

Conflict of Interest

The authors declare no conflict of interest.

[1] M. Armand, J.-M. Tarascon, *Nature* **2008**, *451*, 652–657

[2] Y. Kang, G. Ceder, *Nature* **2009**, *458*, 190–193

[3] B. Dunn, H. Kamath, J.-M. Tarascon, *Science* **2011**, 928–935

[4] A. N. Jansen, A. J. Kahaian, K. D. Kepler, P. A. Nelson, K. Amine, D. W. Dees, D. R. Vissers, M. M. Thackeray, *J. Power Sources* **1999**, *81–82*, 902–905

[5] A. D. Pasquier, I. Plitz, S. Menocal, G. Amatucci, *J. Power Sources* **2003**, *115*, 171–178

[6] J. Chen, *Materials* **2013**, *6,* 156–183

[7] S. Flandrois, B. Simon, *Carbon* **1999**, *37*, 165–180

[8] V. Etacheri, R. Marom, R. Elazari, G. Salitra, D. Aurbach, *Energy Environ. Sci.* **2011**, *4*, 3243–3262

[9] Z. Guo, J. Zhu, J. Feng, S. Du, *RSC Adv.* **2015**, *5*, 69514–69521

[10] B. Moradi, G. G. Botte, *J. Appl. Electrochem.* **2016**, *46*, 123–148

[11] L. Zhao, Y. S. Hu, H. Li, Z. X. Wang, L. Q. Chen, *Adv. Mater.* **2011**, *23,*1385–1388

[12] H. G. Jung, S. T. Myung, C. S. Yoon, S. B. Son, K. H. Oh, K. Amine, B. Scrosati, Y. K. Sun, *Energy Environ. Sci.* **2011**, *4*, 1345–1351

[13] A. R. Armstrong, G. Armstrong, J. Canales, R. Garcia, P. G. Bruce, *Adv. Mater.* **2005**, *17*, 862–865

[14] J. S. Chen, Y. L. Tan, C. M. Li, Y. L. Cheah, D. Y. Luan, S. Madhavi, F. Y. C. Boey, L. A. Archer, X. W. Lou, *J. Am. Chem. Soc.* **2010**, *132*, 6124–6130

[15] A. Jaiswal, C. R. Horne, O. Chang, W. Zhang, W. Kong, E. Wang, T. Chern, M. M. Doeff, *J. Electrochem. Soc.* **2009**, *156*, A1041–A1046

[16] A. Swiderska-Mocek, *Electrochim. Acta* **2014**, *139*, 337–344

[17] J. Liu, W. K. Pang, T. Zhou, L. Chen, Y. Wang, V. K. Peterson, Z. Yang, Z. Guo, Y. Xia, *Energy Environ. Sci.* **2017**, *10*, 1456–1464

[18] J. Liu, Y. Liu, M. Hou, Y. Wang, C. Wang, Y. Xia, *Electrochim. Acta* **2017**, *260*, 695–702

[19] A. K. Padhi, K. S. Nanjundaswamy, J. B. Goodenough, *J. Eletrochem. Soc.* **1997**, *144*, 1188–1194

[20] C. Delacourt, P. Poizot, M. Morcrette, J. -M. Tarascon, C. Masquelier, *Chem. Mater.* **2004**, *16*, 93–99

[21] K. Amine, H. Yasuda, M. Yamachi, *Electrochem. Solid-State Lett.* **2000**, *3*, 178–179

[22] A. Nyten, A. Abouimrane, M. Armand, T. Gustafsson, J. O. Thomas, *Electrochem. Commun.* **2005**, *7*, 156–160

[23] A. Yamada, N. Iwane, Y. Harada, S. Nishimura, Y. Koyama, I. Tanaka, *Adv. Mater.* **2010**, *22*, 3583–3587

[24] Z. Jian, L. Zhao, H. Pan, Y.-S. Hu, H. Li, W. Chen, L. Chen, *Electrochem. Commun.* **2012** *14*, 86–89

[25] L. Chen, J. Y. Liu, Z. W. Guo, Y. G. Wang, C. X. Wang, Y. Y. Xia, *J. Electrochem. Soc.* **2016**, *163*, A904–A910

[26] K. Nakamoto, Y. Kano, A. Kitajou, S. Okada, *J. Power Sources* **2016**, *327*, 327–332

[27] N. A. Milne, C. S. Griffith, J. V. Hanna, M. S. Kazacos, V. Luca, *Chem. Mater.* **2006**, *18*, 3192–3202

[28] Y. Liu, J. Liu, Y. Wu, D. Bin, S.-H. Bo, Y. Wang, Y. Xia, *ACS Appl. Energy Mater* **2018**, *1*, 5151–5157

[29] A. Ziadi, H. Hillebrecht, G. Thiele, B. Elouadi, *J. Solid State Chem.* **1996**, *123*, 324–330

[30] R. Yazami, *Electrochim. Acta* **1999**, *45*, 87–97

[31] S. Yoona, H. Kimb, S. M. Oh, *J. Power Sources* **2001**, *94*, 68–73

[32] H. Kobayashi, Y. Arachi, H. Kageyamaa, K. Tatsumia, *J. Mater. Chem.* **2004**, *14*, 40–42

[33] Y. Arachi, H. Kobayashi, S. Emura, Y. Nakata, M. Tanaka, T. Asai, H. Sakaebe, K. Tatsumi, H. Kageyama, *Solid State Ionics* **2005**, *176*, 895–903

[34] S. Nishimura, G. Kobayashi, K. Ohoyama, R. Kanno, M. Yashima, A. Yamada, *Nat. Mater.* **2008**, *7*, 707–711

[35] N. Igawa, T. Taguchi, H. Fukazawa, H. Yamauchi, W. Utsumi, *J. Am. Ceram. Soc.* **2010**, *93*, 2144–2146

[36] Y. Kato, S. Hori, T. Saito, K. Suzuki, M. Hirayama, A. Mitsui, M. Yonemura, H. Iba, R. Kanno, *Nat. Energy* **2016**, DOI: 10.1038/NENERGY.2016.30

[37] C. Dietrich, D. A. Weber, S. Culver, A. Senyshyn, S. J. Sedlmaier, S. Indris, J. Janek, W. G. Zeier, *Inorg. Chem.* **2017**, *56*, 6681–6687

[38] T. Ohzuku, A. Ueda, N. Yamamota, *J. Electrochem. Soc.* **1995**, *142*, 1431–1435

[39] S. Scharner, W. Weppner, P. Schmid-Beurmann, *J. Electrochem. Soc.* **1999**, *146*, 857–861

[40] S. Panero, P. Reale, F. Ronci, B. Scrosati, P. Perfetti, V. Rossi Albertini, *Phys. Chem. Chem. Phys.* **2001**, *3*, 845–847

[41] S. Li, J. Guo, Z. Ye, X. Zhao, S. Wu, J.-X. Mi, C.-Z. Wang, Z. Gong, M. J. McDonald, Z. Zhu, K.-M. Ho, Y. Yang, *ACS Appl. Mater. Interfaces* **2016**, *8*, 17233–17238

[42] H. Zhang, D. Buchholz, S. Passerini, *Energies* **2017**, *10*, 889

[43] Y. Wang, X. Yu, S. Xu, J. Bai, R. Xiao, Y.-S. Hu, H. Li, X.-Q. Yang, L. Chen, X. Huang, *Nat. Commun.* **2013**, *4*, 2365

[44] S. Adams, *Solid State Ionics* **2006**, *177*, 1625–1630

[45] S. Adams, R. P. Rao, *Phys. Chem. Chem. Phys.* **2009**, *11*, 3210–3216

[46] R. B. -Hadjean, L. T. N. Huynh, N. Emery, J. P. Pereira-Ramos, *Electrochim. Acta* **2018**, *270*, 224–235

[47] F. Strauss, G. Rousse, D. A. D. Corte, M. B. Hassine, M. Saubanere, M. Tang, H. Vezin, M. Courty, R. Dominkoae, J.-M. Tarascon, *Phys. Chem. Chem. Phys.* **2016**, *18*, 14960–14969

[48] L. Lander, M. Reynaud, J. Carrasco, N. A. Katcho, C. Bellin, A. Polian, B. Baptiste, G. Rousseabc, J.-M. Tarascon, *Phys. Chem. Chem. Phys.* **2016**, *18*, 14509–14519

[49] Z. Huang, Z. Wang, Q. Jing, H. Guo, X. Li, Z. Yang, *Electrochim. Acta* **2016**, *192*, 120–126

[50] X. Yang, A. L. Rogach, *Adv. Energy Mater.* **2019**, 1900747